Rheological Behavior of Polymer Blends

HSIAO-KEN CHUANG and CHANG DAE HAN, *Department of Chemical Engineering, Polytechnic Institute of New York, Brooklyn, New York 11201*

Synopsis

Steady and oscillatory shearing flow properties of compatible and incompatible polymer blend systems were measured, using a cone-and-plate rheometer. The compatible blend systems investigated are blends of two low-density polyethylenes (LDPE) having different values of molecular weight and blends of poly(methyl methacrylate) (PMMA) with poly(vinylidene fluoride) (PVDF). The incompatible blend system investigated is a blend of poly(methyl methacrylate) (PMMA) with polystyrene (PS). It was found that (1) plots of first normal stress difference ($\tau_{11} - \tau_{22}$) vs. shear stress (τ_{12}) and plots of storage modulus (G') vs. loss modulus (G'') for the LDPE blends become independent of temperature and blend composition; (2) plots of $\tau_{11} - \tau_{22}$ vs. τ_{12}, and G' vs. G'' for the PMMA/PVDF blends become independent of temperature but dependent upon blend composition. It was found further that, for the incompatible PMMA/PS blends, the dependence of $\tau_{11} - \tau_{22}$ on blend composition, when plotted against τ_{12}, is different from the dependence of G' on blend composition, when plotted against G''. However, in both compatible and incompatible blend systems, plots of $\tau_{11} - \tau_{22}$ vs. τ_{12} and plots of G' versus G'' are independent of temperature. The seemingly complicated composition-dependent rheological behavior of the incompatible blend system is explained with the aid of photomicrographs describing the state of dispersion.

INTRODUCTION

Broadly classified, there are two types of polymer blends: heterogeneous (i.e., immiscible or incompatible) blends and homogeneous (i.e., miscible or compatible) blends. Homogeneous blends give rise to a single phase in which individual components are mutually soluble in one another. The properties of these blends usually obey the rule of mixtures, although, sometimes, physical/mechanical properties superior to those of the individual components have been observed.

On the other hand, heterogeneous polymer blends can have two different types of dispersion state: (1) One component forms a continuous phase and the other component forms a discrete phase; (2) the individual components each form continuous phases, giving rise to an *interlocked* or *interpenetrated* state of dispersion. At present, unfortunately, there is no theory that predicts which of the two components will form a continuous (or discrete) phase, or whether both will, when two incompatible polymers are blended, although there have been some guidelines suggested on the basis of theoretical[1] and somewhat limited experimental investigations.[2,3]

It has been amply demonstrated in the literature[1–10] that, when dealing with a heterogeneous polymer blend, the morphology of the blend (e.g., the state of dispersion, domain size, and its distribution) controls its rheological properties. It is important to point out that the method of blend preparation (e.g., the method of mixing the polymers, the intensity of mixing) and the variables chosen for blend preparation (e.g., temperature, blend composition, shear stress) strongly

Journal of Applied Polymer Science, Vol. 29, 2205–2229 (1984)

CCC 0021-8995/84/062205-25$04.00

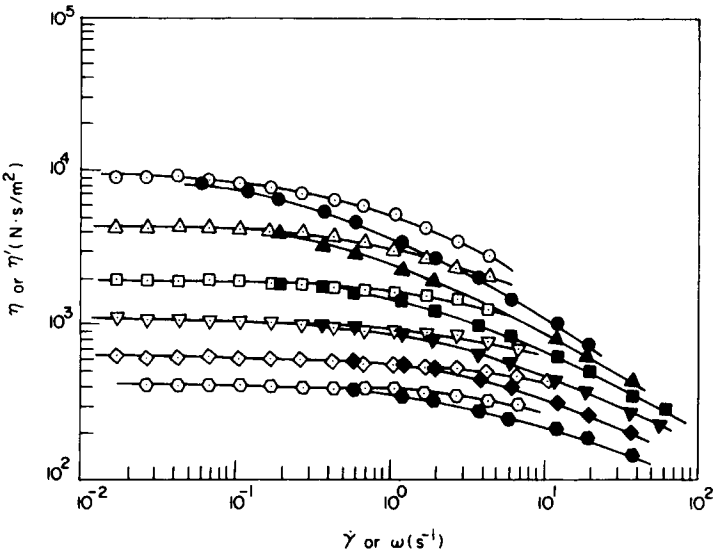

Fig. 1. η vs. $\dot{\gamma}$ (open symbols) and η' vs. ω (closed symbols) at 160°C for LDPE homopolymers and their blends: (⊙,●) MN722; (⊙,●) MN714; (△,▲) MN722/MN714=80/20; (⊡,■) MN722/MN714=60/40; (▽,▼) MN722/MN714=40/60; (◇,◆) MN722/MN714=20/80.

influence the morphology and, therefore, the rheological properties of the blend. It is then clear that the rheological behavior of heterogeneous polymer blends can be understood correctly only when information on the morpohology is available.

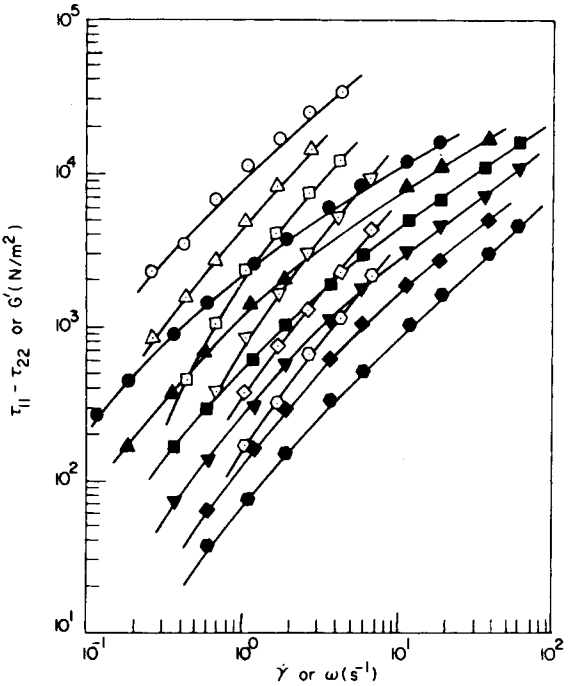

Fig. 2. $\tau_{11} - \tau_{22}$ vs. $\dot{\gamma}$ and G' vs. ω at 160°C for LDPE homopolymers and their blends. Symbols are the same as in Figure 1.

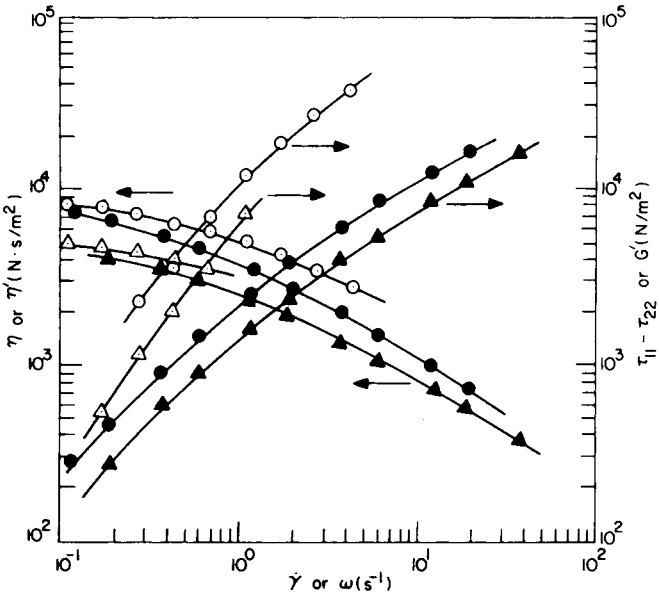

Fig. 3. η and $\tau_{11} - \tau_{22}$ vs. $\dot{\gamma}$ (open symbols) and η' and G' vs. ω (closed symbols) for MN722 at two different temperatures (°C): (⊙,●) 160; (△,▲) 180.

As part of our continuing effort on enhancing our understanding of the rheological behavior of polymer blends, we have chosen two compatible and one incompatible polymer systems and investigated their rheological behavior. For the incompatible blend system, we have also investigated its morphological states. This helped us to interpret the rheological properties independently determined. In this paper we shall report the highlights of our findings.

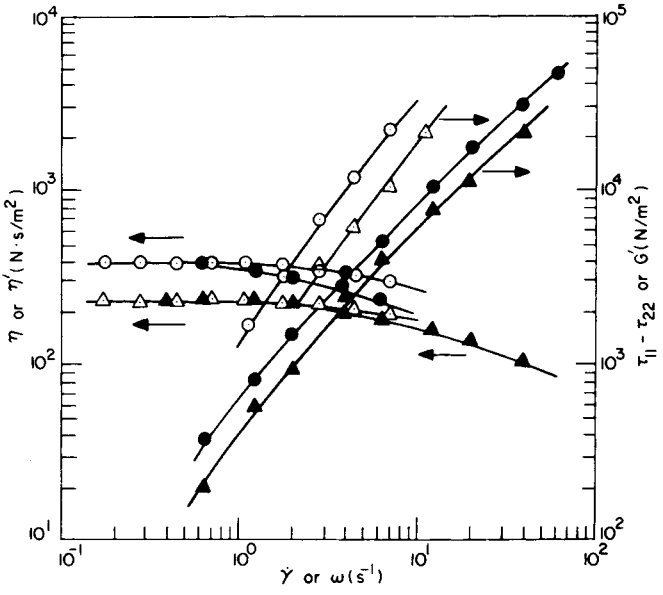

Fig. 4. η and $\tau_{11} - \tau_{22}$ vs. $\dot{\gamma}$, and η' and G' vs. ω, for MN714. Symbols are the same as in Figure 3.

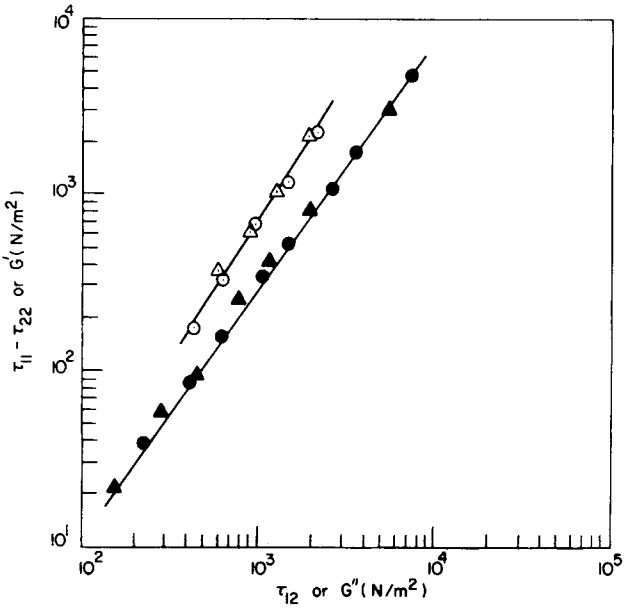

Fig. 5. $\tau_{11} - \tau_{22}$ vs. τ_{12} (open symbols) and G' vs. G' (closed symbols) for MN714 at two temperatures (°C): (⊙,●) 160; (△,▲) 180.

EXPERIMENTAL

Materials. We have prepared the following blend systems: (1) blends of two low-density polyethylenes (LDPE) (U.S. Industrial Chemical Co., MN714 and MN722) having different values of molecular weight; (2) blends of poly-

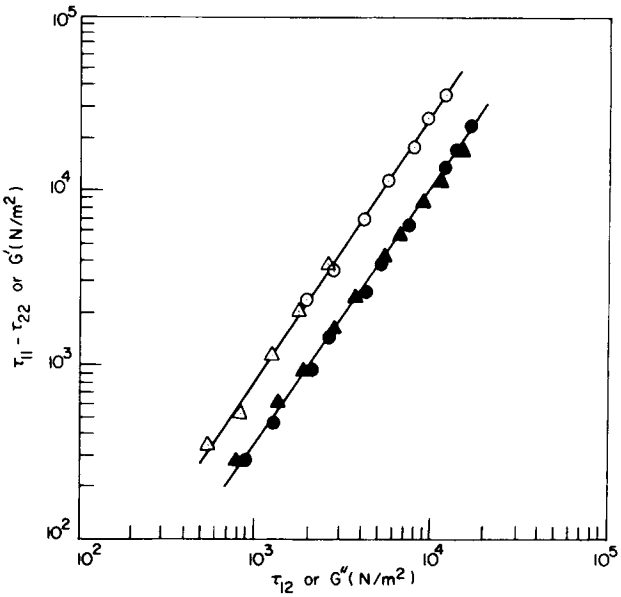

Fig. 6. $\tau_{11} - \tau_{22}$ vs. τ_{12} and G' vs. G'' for MN722. Symbols are the same as in Figure 5.

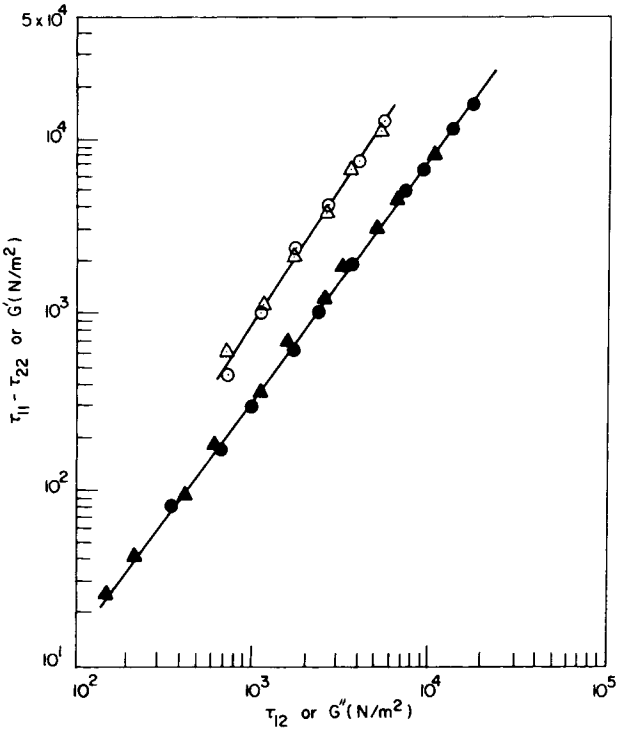

Fig. 7. $\tau_{11} - \tau_{22}$ vs. τ_{12} and G' vs. G'' for the MN722/MN714=60/40 blend. Symbols are the same as in Figure 5.

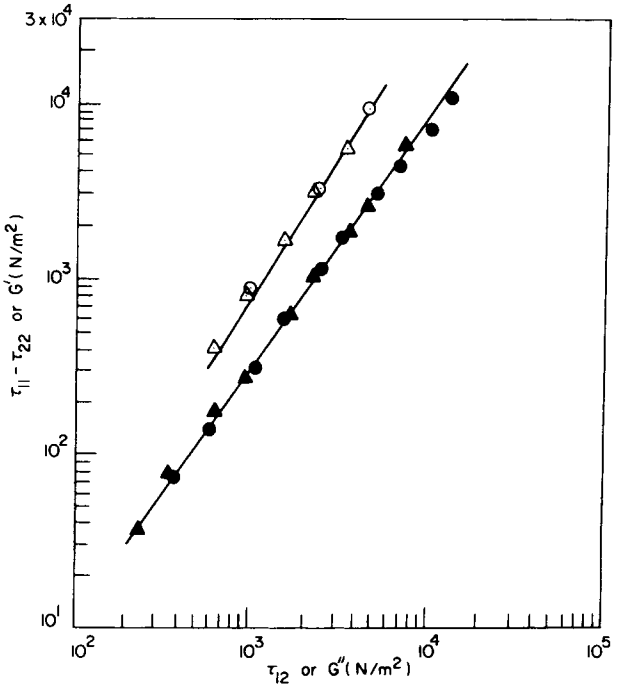

Fig. 8. $\tau_{11} - \tau_{22}$ vs. τ_{12}, and G' vs. G'' for the MN722/MN714=40/60 blend. Symbols are the same as in Figure 5.

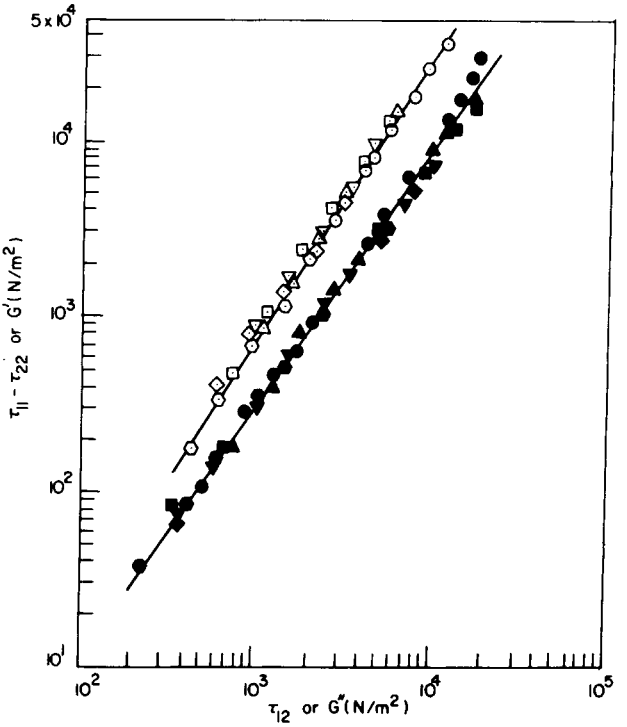

Fig. 9. $\tau_{11} - \tau_{22}$ vs. τ_{12} (open symbols) and G' vs. G'' (closed symbols) at 160°C for LDPE homopolymers and their blends: (⊙,●) MN722; (⊙,●) MN714; (△,▲) MN722/MN714=80/20; (⊡,■) MN722/MN714=60/40; (▽,▼) MN722/MN714=40/60; (◇,◆) MN722/MN714=20/80.

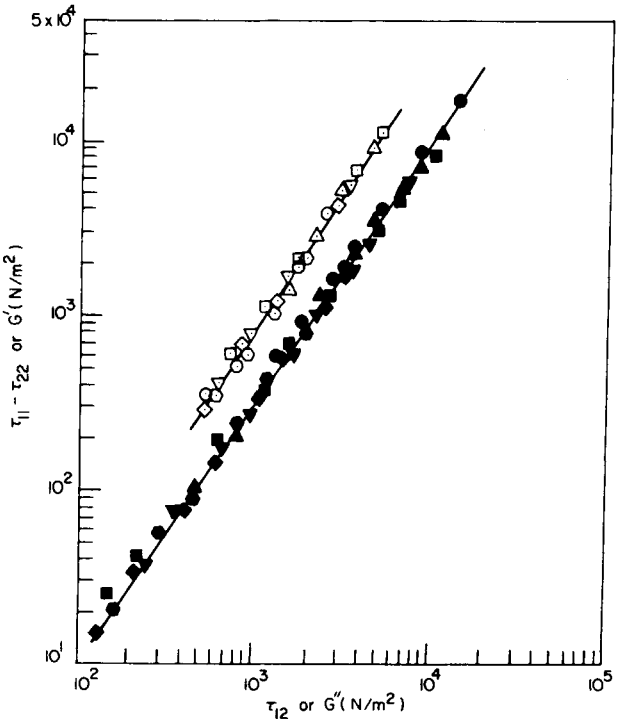

Fig. 10. $\tau_{11} - \tau_{22}$ vs. τ_{12} and G' vs. G'' at 180°C for LDPE homopolymers and their blends. Symbols are the same as in Figure 9.

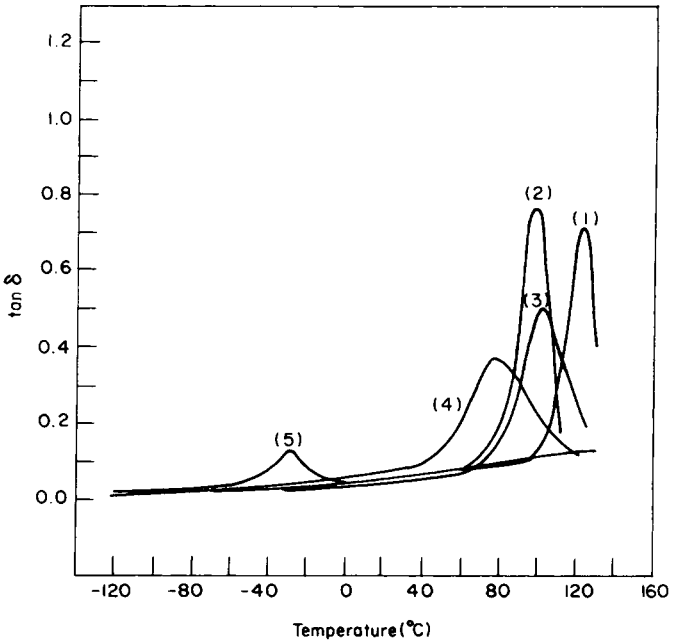

Fig. 11. Loss tangent vs. temperature for: (1) PMMA; (2) PMMA/PVDF=70/30; (3) PMMA/PVDF=50/50; (4) PMMA/PVDF=30/70; (5) PVDF.

(methyl methacrylate) (PMMA) (Rohm and Haas, Plexiglas V920) and poly-(vinylidene fluoride) (PVDF) (Pennwalt, Kynar 951); (3) blends of poly(methyl methacrylate) (PMMA) (Rohm and Haas, Plexiglas V920) and polystyrene (PS) (Dow Chemical, STYRON 685D).

The reasons for the choice of these blend systems are as follows. First, there

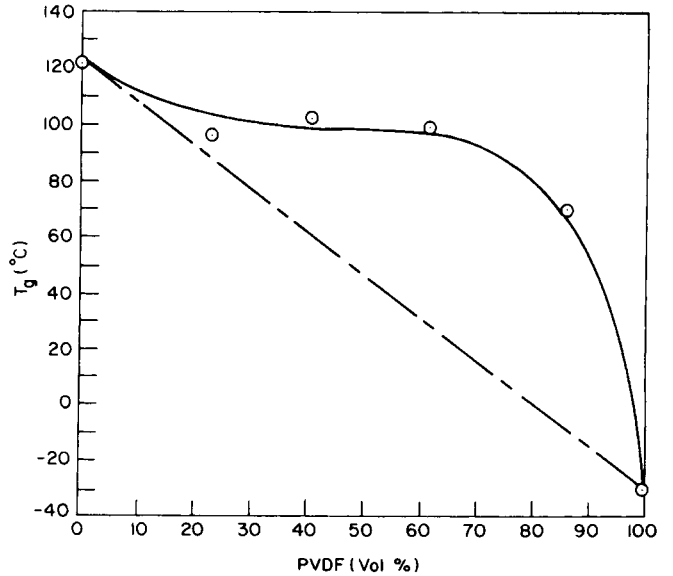

Fig. 12. Glass transition temperature vs. vol % of PVDF in the PMMA/PVDF blend system.

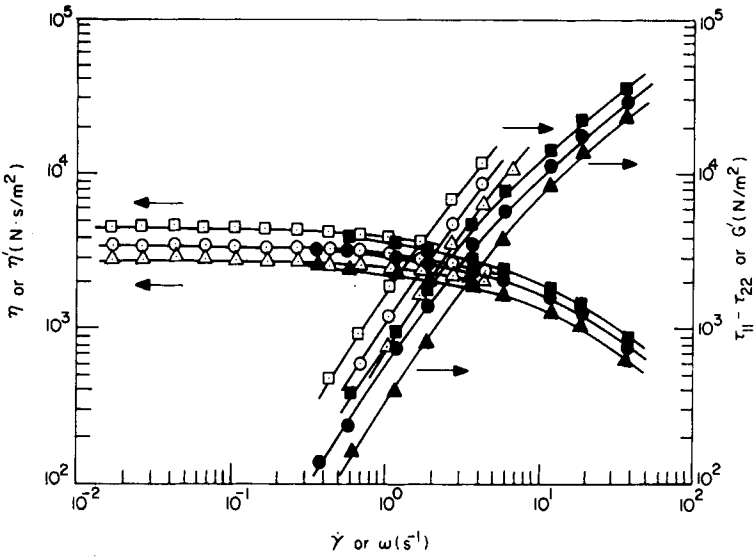

Fig. 13. η and $\tau_{11} - \tau_{22}$ vs. $\dot{\gamma}$ (open symbols) and η' and G' vs. ω (closed symbols) for PVDF at three different temperatures (°C): (⊡,■) 210; (⊙,●) 220; (△,▲) 230.

is no doubt about the compatibility of the LDPE blends. Therefore, this blend system can serve as a reference for interpreting the rheological behavior of the other blend systems investigated. Second, the PMMA/PVDF blend system has long been known to be compatible.[11–15] We have found that, when coextruded to produce two-layer films, the adhesion was so strong, that we could not separate the individual layers. Unfortunately, its rheological behavior has *not* been re-

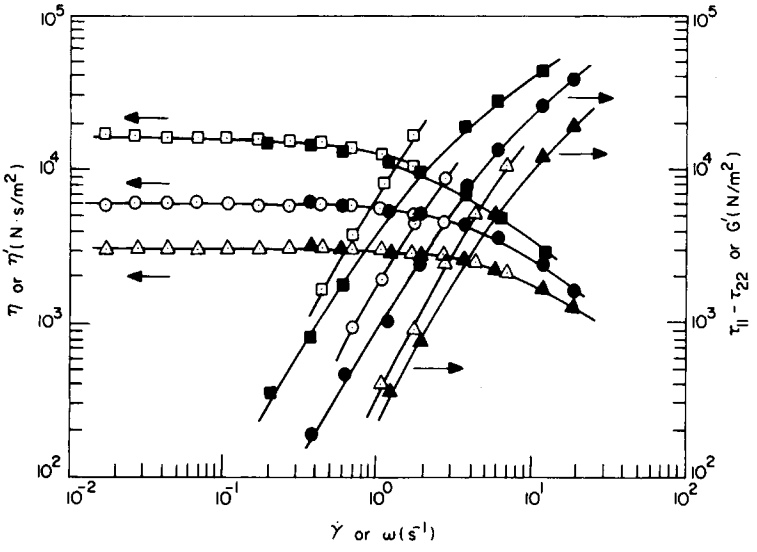

Fig. 14. η and $\tau_{11} - \tau_{22}$ vs. $\dot{\gamma}$ and η' and G' vs. ω for PMMA. Symbols are the same as in Figure 13.

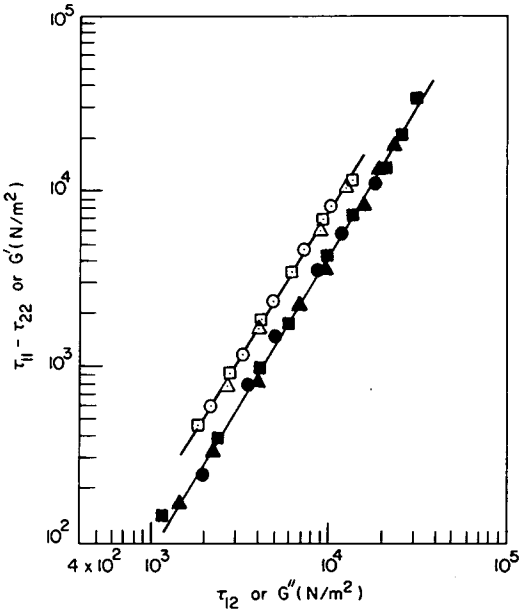

Fig. 15. $\tau_{11} - \tau_{22}$ vs. τ_{12} (open symbols) and G' vs. G'' (closed symbols) for PVDF at different temperatures (°C): (⊡,■) 210; (⊙,●) 220; (△,▲) 230.

ported in the literature. Third, the PMMA/PS blend system was chosen, because this system has been known to be incompatible and, moreover, the same PMMA was also used in the compatible PMMM/PVDF blend system.

Preparation of the Blends Investigated. The LDPE blends were prepared

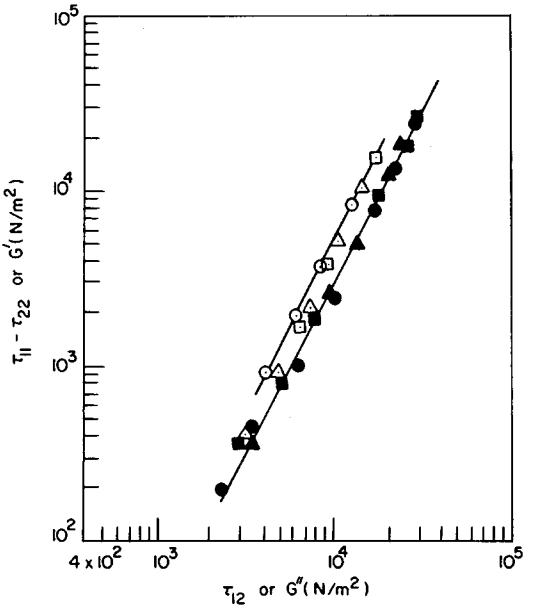

Fig. 16. $\tau_{11} - \tau_{22}$ vs. τ_{12} and G' vs. G'' for PMMA. Symbols are the same as in Figure 15.

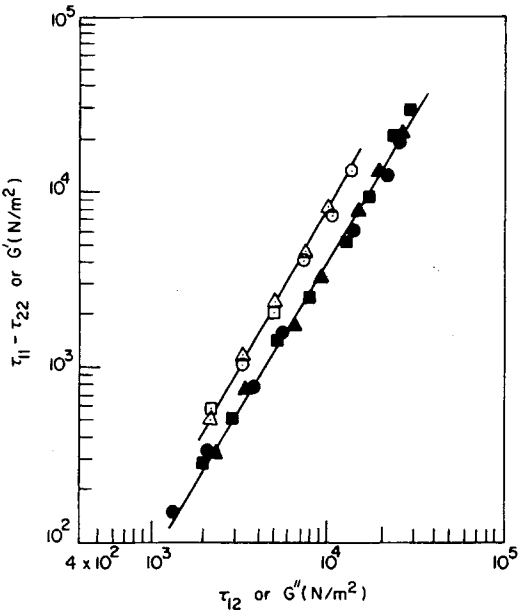

Fig. 17. $\tau_{11} - \tau_{22}$ vs. τ_{12} and G' vs. G'' for the PVDF/PMMA=40/60 blend. Symbols are the same as in Figure 15.

by tumbling mixtures of two polymers (MN714 and MN722) available in the form of powder. Since the amount of each blend prepared was small, we believe that mixing by tumbling was sufficient to achieve a homogeneous dispersion of the

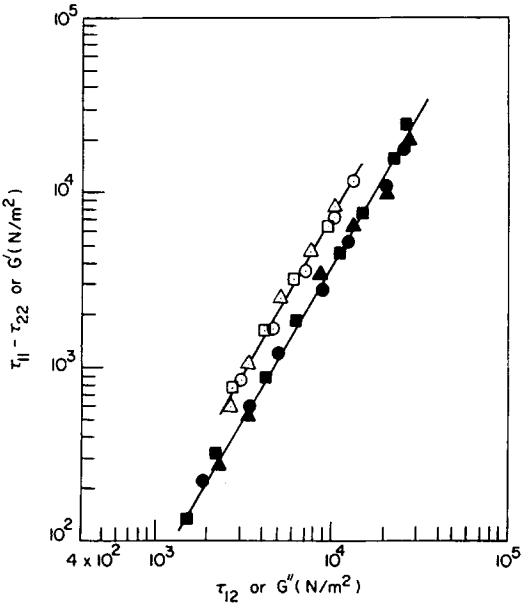

Fig. 18. $\tau_{11} - \tau_{22}$ vs. τ_{12} and G' vs. G'' for the PVDF/PMMA=60/40 blend. Symbols are the same as in Figure 15.

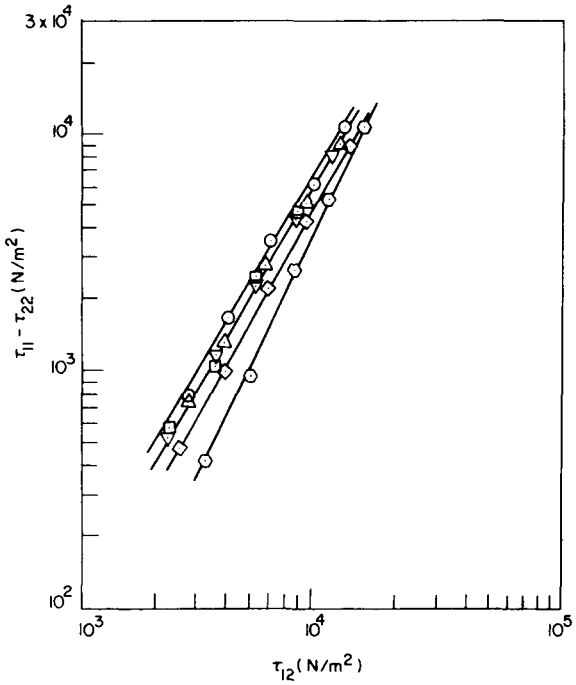

Fig. 19. $\tau_{11} - \tau_{22}$ vs. τ_{12} at 230°C for the PVDF/PMMA blend system: (⊙) PVDF; (⊙) PMMA, (△) PVDF/PMMA=80/20; (□) PVDF/PMMA=60/40; (▽) PVDF/PMMA=40/60; (◇) PVDF/PMMA=20/80.

two components. The blend ratios chosen were 20/80, 40/60, 60/40, and 80/20 by weight.

The two other blend systems (PMMA/PVDF; PMMA/PS) were prepared by using a twin-screw compounding machine (Werner and Pfleiderer, ZDSK-53). The mixing of the material was achieved by conveying and kneading with screw bushings and kneading elements assembled in the machine. The material was discharged through a die plate and into a water bath. The strands quenched in the water bath were then cut into pellets. Various blend ratios were chosen for each system.

Rheological Measurement. The compounded pellets were compression-molded into disks, 2 cm in diameter and 3 mm thick, using a hydraulic press.

A cone-and-plate rheometer (a Weissenberg Model R-16 Rheogoniometer) was used to measure (1) steady shearing flow properties, namely viscosity (η), shear stress (τ_{12}), and first normal stress difference ($\tau_{11} - \tau_{22}$), and (2) oscillatory shearing flow properties, namely, dynamic viscosity (η'), storage modulus (G'), and loss modulus (G''). These quantities were determined using the expressions described in the literature.[16,17]

RESULTS

Blends of Two Low-Density Polyethylenes. Figure 1 gives plots of η vs. shear rate ($\dot{\gamma}$) and η' vs. frequency (ω), and Figure 2 gives plots of $\tau_{11} - \tau_{22}$ vs. shear rate ($\dot{\gamma}$) and G' vs. frequency (ω) for the LDPE blends investigated. Figures 3 and 4 give plots of η and $\tau_{11} - \tau_{22}$ vs. $\dot{\gamma}$, and η' and G' vs. ω, for MN722

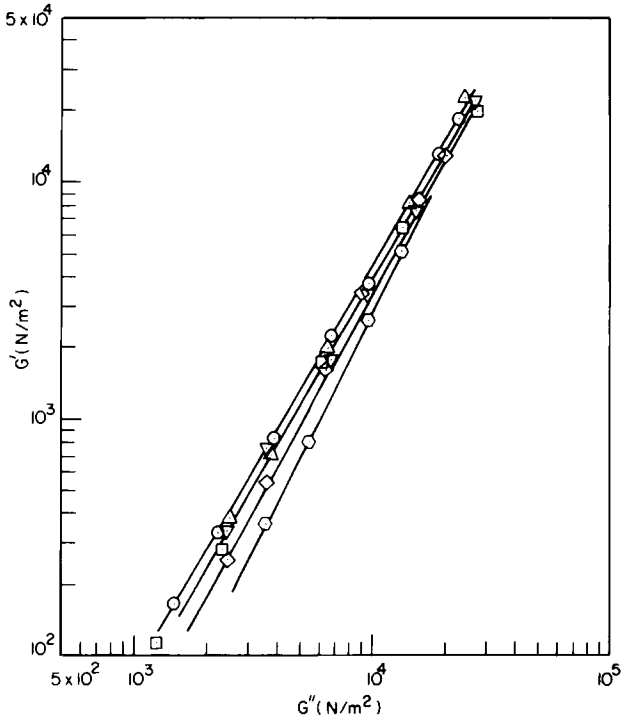

Fig. 20. G' vs. G'' at 230°C for the PVDF/PMMA blend system. Symbols are the same as in Figure 19.

and MN714, respectively, at two different temperatures, 160°C and 180°C. It is seen in Figures 3 and 4 that both $\tau_{11} - \tau_{22}$ and G' decrease with increasing temperature. However, when $\tau_{11} - \tau_{22}$ is plotted against τ_{12}, and G' against G'', the dependence of $\tau_{11} - \tau_{22}$ and G' on temperature is suppressed, as may be seen in Figures 5–8. This observation is consistent with that reported by Han and Lem.[18]

Figure 9 gives plots of $\tau_{11} - \tau_{22}$ vs. τ_{12}, and G' vs. G'', for the homopolymers and blends investigated, at 160°. Similar plots are given in Figure 10 at 180°C. Three things are worth elaborating on: (1) a single correlation ($\tau_{11} - \tau_{22}$ vs. τ_{12} and G' vs. G'') is obtained, regardless of whether the material is homopolymer or blend; (2) the correlation obtained is independent of the temperature at which rheological measurements were taken; (3) the magnitude of $\tau_{11} - \tau_{22}$ is greater than that of G' by a factor of 2–3, depending on the range of τ_{12} (or G'') investigated. More specifically stated, at low values of τ_{12} or G'', we have the following relationship:

$$\lim_{\dot{\gamma}\to 0} \frac{\tau_{11} - \tau_{22}}{\dot{\gamma}^2} = \lim_{\omega\to 0} \frac{2G'}{\omega^2} \tag{1}$$

consistent with the theoretical prediction.

What are most remarkable are the correlations, given in Figures 9 and 10, demonstrating that the dependency of $\tau_{11} - \tau_{22}$ and G' on blend composition disappears. This then suggests that the blends of MN714 and MN722 having different molecular weights (MW) and molecular weight distributions (MWD)

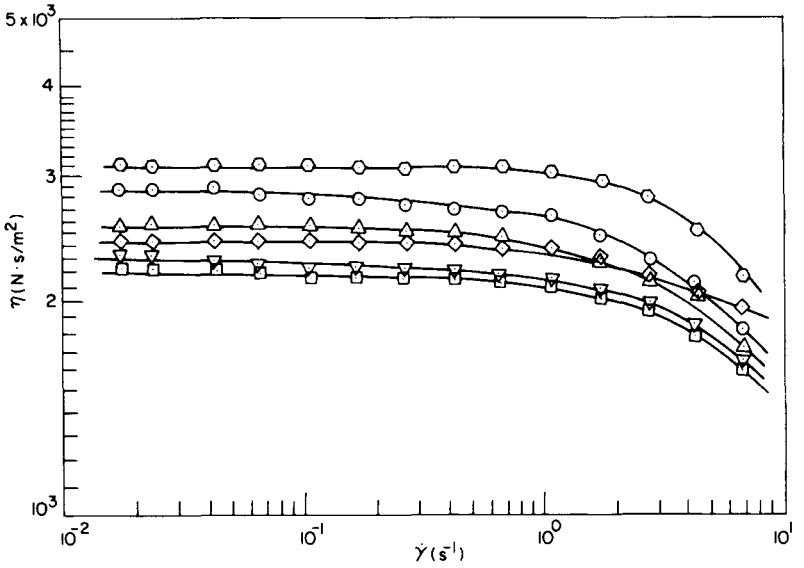

Fig. 21. η vs. $\dot{\gamma}$ at 230°C for the PVDF/PMMA blend system. Symbols are the same as in Figure 19.

behave as if they were homopolymers, which is attributable to their compatibility.

Blends of Poly(methyl Methacrylate) (PMMA) and Poly(vinylidene Fluoride) (PVDF). Blends of PMMA and PVDF are known to be compatible on the basis of the glass transition temperature T_g, as may be seen in Figure 11. Figure 12 gives plots of T_g vs. blend composition. It is seen that the T_g's of the PMMA/PVDF blends do not follow the additivity rule,

$$T_g = w_1 T_{g1} + w_2 T_{g2} \tag{2}$$

Figures 13 and 14 give plots of η and $\tau_{11} - \tau_{22}$ vs. $\dot{\gamma}$, and η' and G' vs. ω, at three different temperatures (210°C, 220°C, and 230°C) for PVDF and PMMA, respectively. It is seen that η and η' decrease with increasing temperature, and $\tau_{11} - \tau_{22}$ and G' also decrease with increasing temperature. When $\tau_{11} - \tau_{22}$ is plotted against τ_{12}, and G' against G'', as shown in Figures 15–18, a temperature-independent correlation is obtained.

Figure 19 gives plots of $\tau_{11} - \tau_{22}$ vs. τ_{12}, and Figure 20 plots of G' vs. G'', for the homopolymers and blends investigated, at 230°C. It is seen in Figures 19 and 20 that, in contrast to the LDPE blend system investigated (see Figs. 9 and 10), the PVDF/PMMA blend system exhibits a composition-dependent correlation, although the blend system is believed to be compatible on the basis of the glass transition temperature (see Fig. 11).

Figure 21 describes the dependence of η on blend composition, and Figure 22 the dependence of η' on blend composition at 230°C for the PVDF/PMMA blend system. It is seen that the viscosities of the PVDF-rich blends are lower than those of the constituent homopolymers. In view of the fact that PVDF is compatible with PMMA, which is judged from the experimentally observed T_g values

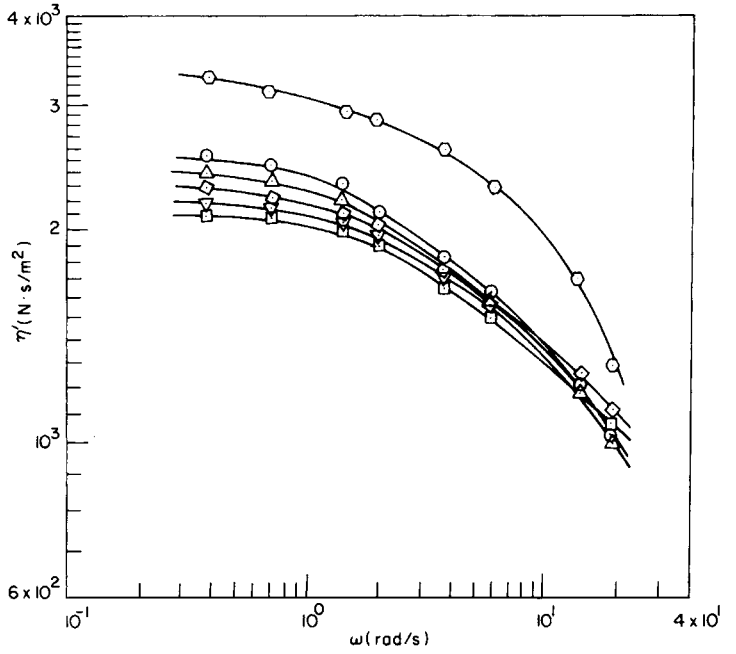

Fig. 22. η' vs. ω at 230°C for the PVDF/PMMA blend system. Symbols are the same as in Figure 19.

(see Fig. 11), one would expect that the viscosities of the PVDF/PMMA blends would lie between those of the PVDF and PMMA.

Blends of Poly(methyl Methacrylate) (PMMA) and Polystyrene (PS). Figures 23–25 give plots of η and $\tau_{11} - \tau_{22}$ vs. $\dot{\gamma}$, and η' and G' vs. ω, at three

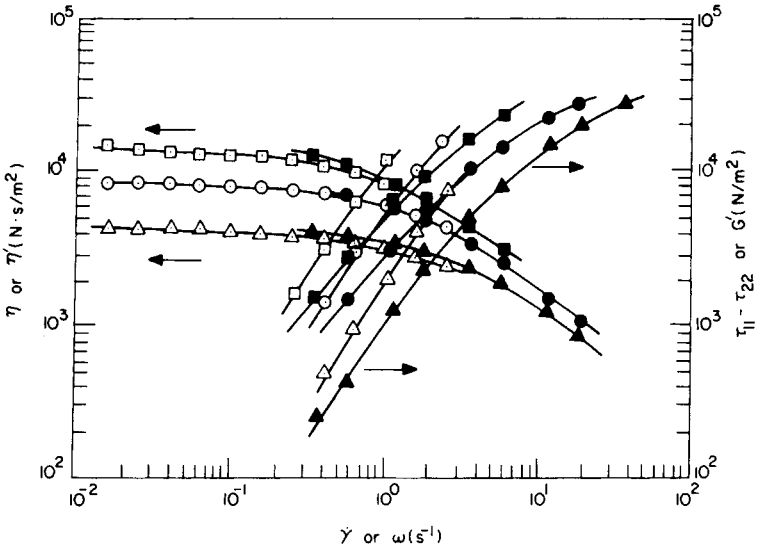

Fig. 23. η and $\tau_{11} - \tau_{22}$ vs. $\dot{\gamma}$ (open symbols) and η' and G'' vs. ω (closed symbols) for PS at three different temperatures (°C): (□,■) 210; (○,●) 220; (△,▲) 230.

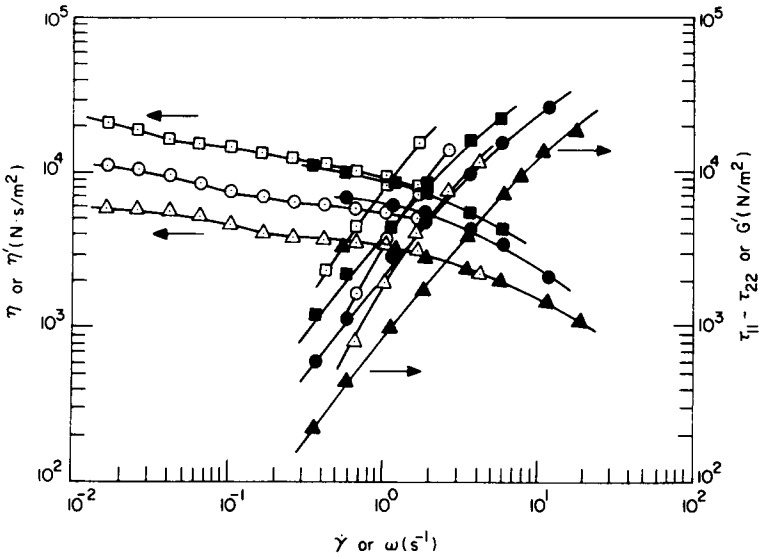

Fig. 24. η and $\tau_{11} - \tau_{22}$ vs. $\dot{\gamma}$ and η' and G' vs. ω for the PS/PMMA=30/70 blend. Symbols are the same as in Figure 23.

different temperatures (210°C, 220°C, 230°C) for PS, the PS/PMMA=30/70 blend, and the PS/PMMA=70/30 blend, respectively (see Fig. 14 for PMMA.) Figures 26–28 give plots of $\tau_{11} - \tau_{22}$ vs. τ_{12}, and G' vs. G'', for the same materials (see Fig. 16 for PMMA). It is seen that such plots give rise to a temperature-independent correlation.

Figure 29 gives plots of $\tau_{11} - \tau_{22}$ vs. τ_{12}, and Figure 30 plots of G' vs. G'', for

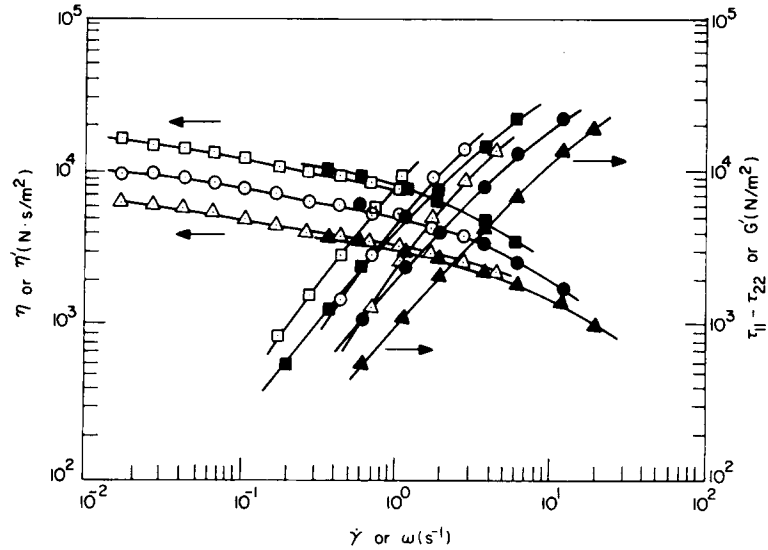

Fig. 25. η and $\tau_{11} - \tau_{22}$ vs. $\dot{\gamma}$ and η' and G' vs. ω for the PS/PMMA=70/30 blend. Symbols are the same as in Figure 23.

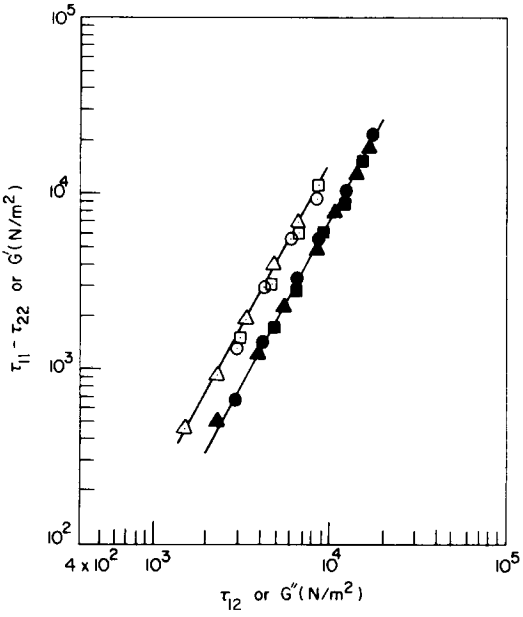

Fig. 26. $\tau_{11} - \tau_{22}$ vs. τ_{12} (open symbols) and G' vs. G'' (closed symbols) for PS at three different temperatures (°C): (⊡,■) 210; (⊙,●) 220; (△,▲) 230.

the homopolymers (PS and PMMA) and their blends investigated. It is seen that plots of $\tau_{11} - \tau_{22}$ vs. τ_{12} do not follow the additivity rule with respect to the blend composition, and that no correlation appears to exist between the steady measurement ($\tau_{11} - \tau_{22}$) and the dynamic measurement (G'), insofar as the blend

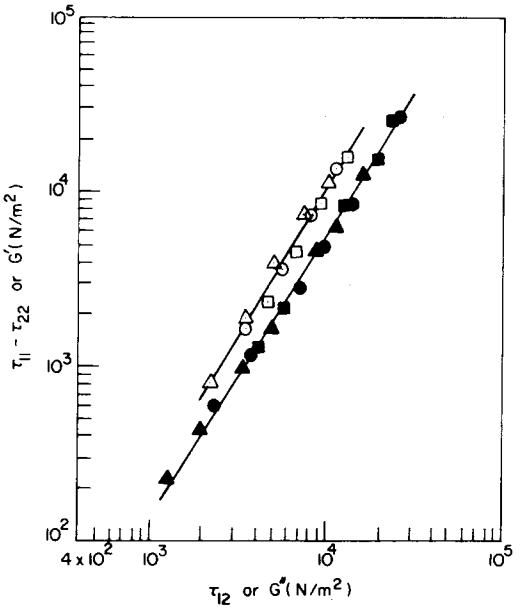

Fig. 27. $\tau_{11} - \tau_{22}$ vs. τ_{12} and G' vs. G'' for the PS/PMMA=30/70 blend. Symbols are the same as in Figure 26.

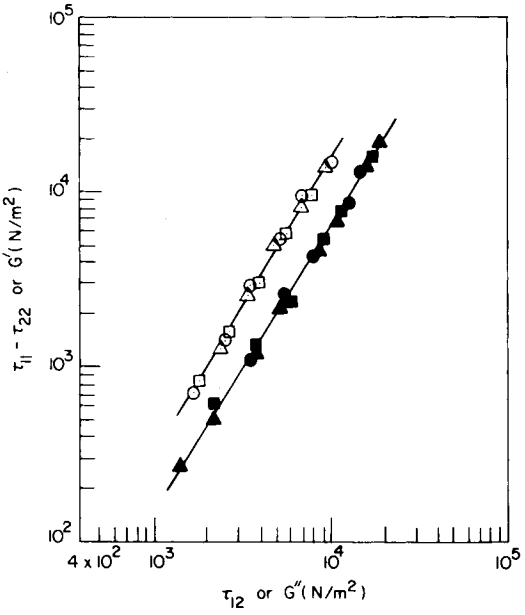

Fig. 28. $\tau_{11} - \tau_{22}$ vs. τ_{12} and G' vs. G'' for the PS/PMMA=70/30 blend. Symbols are the same as in Figure 26.

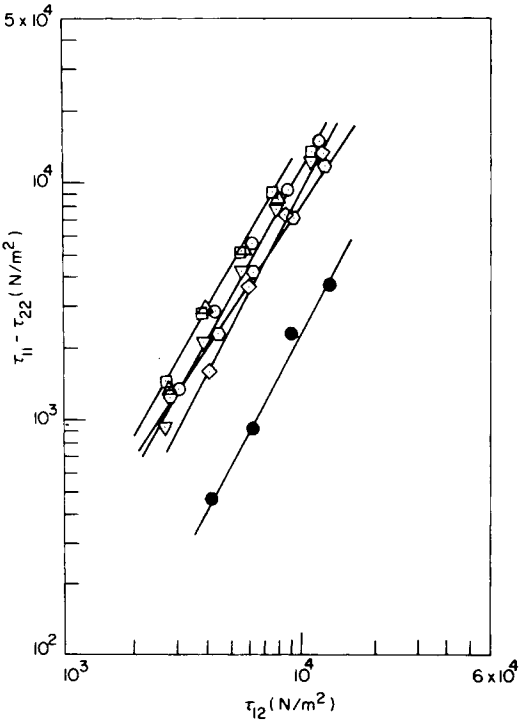

Fig. 29. $\tau_{11} - \tau_{22}$ vs. τ_{12} at 220°C for the PS/PMMA blend system: (⊙) PS; (●) PMMA; (△) PS/PMMA=90/10; (⊡) PS/PMMA=70/30; (▽) PS/PMMA=50/50; (◈) PS/PMMA=30/70; (⊙) PS/PMMA=10/90.

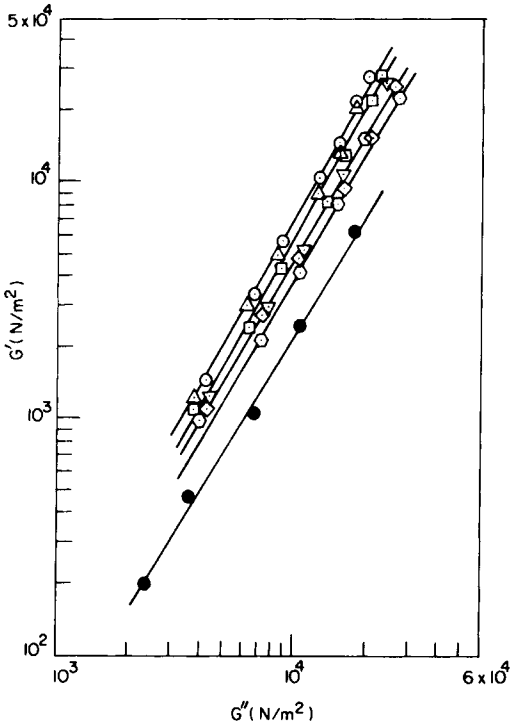

Fig. 30. G' vs. G'' at 220°C for the PS/PMMA blend system. Symbols are the same as in Figure 29.

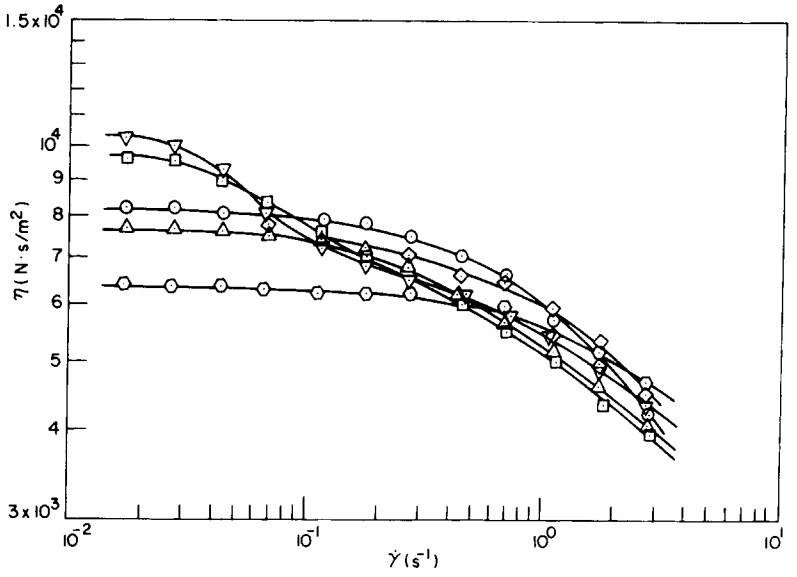

Fig. 31. η vs. $\dot{\gamma}$ at 220°C for the PS/PMMA blend system: (⊙) PS; (⊙) PMMA; (△) PS/PMMA = 90/10; (⊡) PS/PMMA = 70/30; (▽) PS/PMMA = 30/70; (◇) PS/PMMA = 10/90.

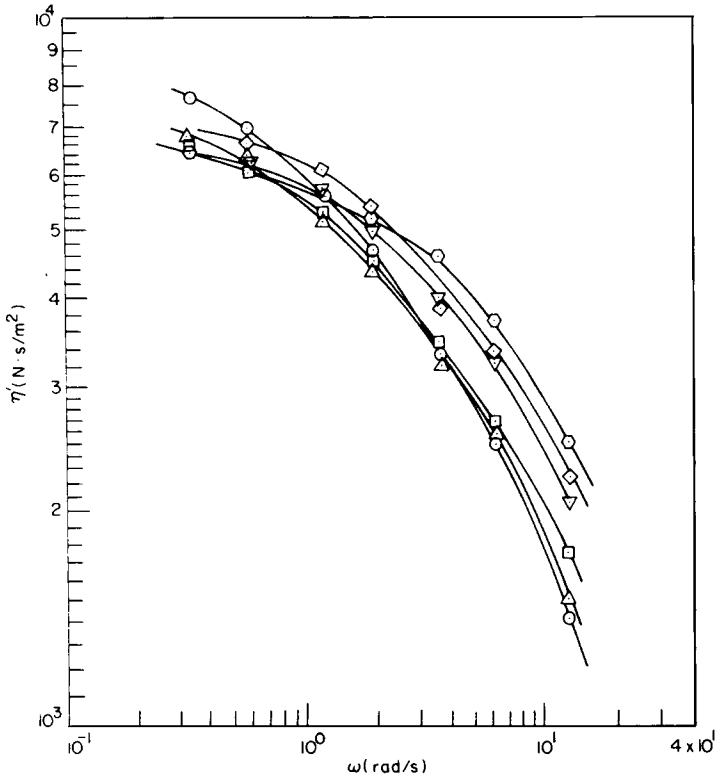

Fig. 32. η' vs. ω at 220°C for the PS/PMMA blend system. Symbols are the same as in Figure 31.

composition is concerned. This observation is quite different from that for the compatible blend systems investigated, namely, the LDPE blend system (see Figs. 9 and 10) and the PMMA/PVDF blend system (see Figs. 19 and 20).

Figure 31 gives plots of η' vs. $\dot{\gamma}$, and Figure 32 displays plots of η' vs. ω, for the PS/PMMA blend system at 220°C. It is seen that the viscosities of the blends cross over as shear rate increases, i.e., the shear dependency of the blend viscosity varies strongly with the blend composition. This may be explained with the aid of the photomicrographs given in Figures 33–37, describing the state of dispersion of the blends. These photomicrographs were taken with a transmission electron microscope. Note in Figures 31 and 32 that no correlation appears to exist between η and η', insofar as the blend composition is concerned.

Note in Figures 33–37 that the *dark* area represents the PS phase and the *white* area the PMMA phase. The following observations are worth noting on the photomicrographs: (1) It appears that the blend composition determines the state of dispersion, i.e., the PS phase forms the discrete phase in the PMMA-rich blend, and the PMMA phase forms the discrete phase in the PS-rich blend. (2) When the specimen was subjected to a steady shearing deformation, the morphological state changed considerably. Note in Figures 31 and 32 that the viscosity ratio of the PS and the PMMA employed varies between 0.5 and 2.0 over the range of shear rates investigated. (3) For the PS/PMMA=10/90 blend, considerable breakage of the PS droplets appears to have occurred while

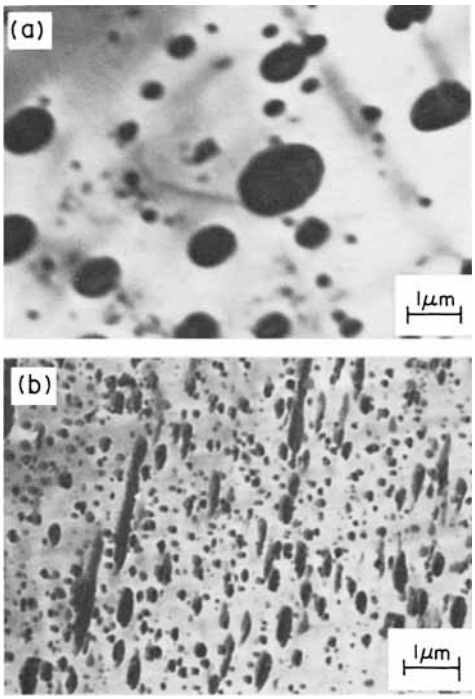

Fig. 33. Photomicrographs for the PS/PMMA = 10/90 blend, in which the *dark* area represents the PS phase and the *white* area represents the PMMA phase: (a) before the specimen was subjected to a shearing motion; (b) after the specimen (T = 220°C) was subjected to a shearing motion at $\dot{\gamma}$ = 2.7 s^{-1}.

the specimen was subjected to a steady shearing deformation. This observation is based on the size of the discrete PS phase dispersed in the PMMA phase, shown in Figure 33. (4) For the PS/PMMA=30/70 blend, shown in Figure 34, the morphological state of the fluid under a steady shearing deformation appears to be somewhat more complex than that of the PS/PMMA=10/90 blend. (5) The state of dispersion of the PS/PMMA=50/50 blend becomes very complex, when subjected to a steady shearing deformation. It is seen in Figure 35 that both the PS and PMMA phases appear to form cocontinuous phases, and in each continuous phase one component is dispersed into the other. This may be explainable by the fact that the blend composition controls the morphological state of the blend, and, in this case, the blend composition is exactly at the border line, i.e., 50/50 blend ratio. (6) For the PS/PMMA=70/30 and PS/PMMA=90/10 blends, the dispersed PMMA phase gives rise to elongated droplets, as may be seen in Figures 36 and 37.

DISCUSSION

Dependence of the Rheological Properties on the Blend Composition

It is demonstrated above that the rheological measurements, especially plots of $\tau_{11} - \tau_{22}$ vs. τ_{12} and plots of G' vs. G'', of polymer blends give different kinds of correlation, depending upon the nature of the compatibility. When a blend

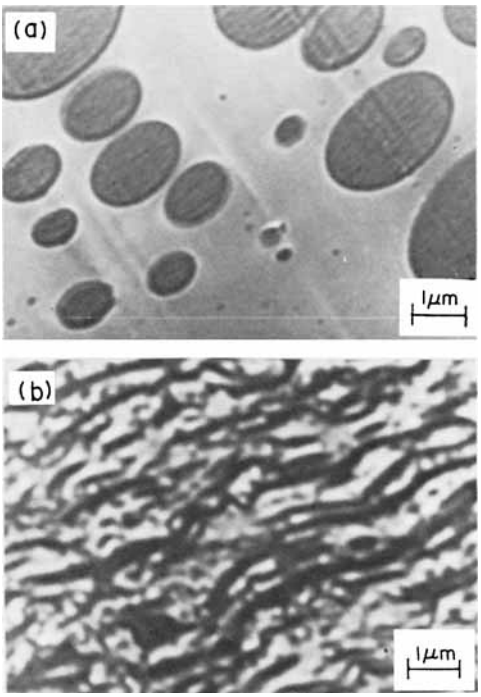

Fig. 34. Photomicrographs for the PS/PMMA = 30/70 blend, in which the *dark* area represents the PS phase and the *white* area represents the PMMA phase: (a) before the specimen was subjected to a shearing motion; (b) after the specimen (T = 220°C) was subjected to a shearing motion at $\dot{\gamma}$ = 2.7 s^{-1}.

system is truly compatible on the molecular level, it gives rise to a composition-independent correlation, when $\tau_{11} - \tau_{22}$ is plotted against τ_{12}, and G' against G''. This was the case with the LDPE blend system investigated. Note that the two different grades of LDPE (MN714 and MN722) have the same molecular structure, and are expected to be compatible on the molecular level. Therefore, any blend of a given composition may be considered to be simply another grade of LDPE.

It should be remembered that τ_{12} and G'' may be interpreted as the energy dissipated and $\tau_{11} - \tau_{22}$ and G'' may be interpreted as the energy stored in the molecules during the shearing deformation. Therefore, as long as the molecular structure is kept the same, the ratio of the energy stored and the energy dissipated during the shearing deformation is expected to be independent of blend composition. For the LDPE blend system investigated, the intuitive expectation is borne out.

On the other hand, the PMMA/PVDF blend system, which is believed to be compatible, gives rise to a composition-dependent correlation when $\tau_{11} - \tau_{22}$ is plotted against τ_{12}, and G' against G''. Figures 19 and 20 show that the dependency of $\tau_{11} - \tau_{22}$ on blend composition is the same as the dependency of G' on blend composition. In other words, the steady shearing flow properties correlate in the same manner as the oscillatory shearing flow properties, insofar as the blend composition is concerned.

Whereas the viscosities (both η and η') of the LDPE blends (see Fig. 1) lie

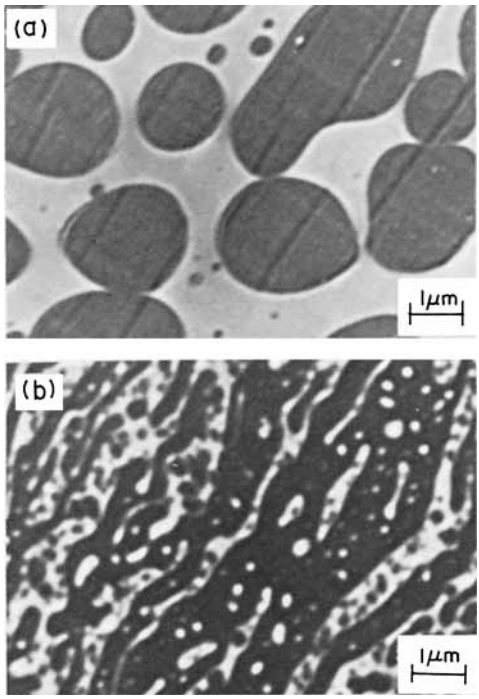

Fig. 35. Photomicrographs for the PS/PMMA=50/50 blend, in which the *dark* area represents the PS phase and the *white* area represents the PMMA phase: (a) before the specimen was subjected to a shearing motion; (b) after the specimen (T = 220°C) was subjected to a shearing motion at $\dot{\gamma}$ = 2.7 s^{-1}.

between those of the constituent components, the viscosities of some blends in the PMMA/PVDF system are lower than those of the constituent components (see Fig. 21). It should be mentioned at this juncture that Han[6–8] has reported viscosity behavior of incompatible blend systems, very similar to that shown in Figure 21, but at much higher shear rates. They explained this rather unusual viscosity behavior on the basis of the deformability of the dispersed phase (i.e., droplets), when subjected to large shear rates. Note, however, that the viscosity reduction observed with the PMMA/PVDF system, shown in Figure 21, occurs at very low shear rates and, moreover, the blends of PMMA and PVDF are believed to be compatible. Therefore, the viscosity reduction observed with the compatible PMMA/PVDF blend system must have an origin quite different from that with incompatible blend systems.

We speculate that a mixture of two different molecular structures, though miscible with each other on the molecular level, can have molecular entanglements which, under a shearing deformation, may give a resistance (or frictional force) less than that which the molecular entanglements of the constituent components may give. Such a speculation should be proved or disproved, using a theory of molecular rheology. This is beyond the scope of the present investigation.

Since the PMMA/PS blend system is incompatible, as demonstrated in Figures 33–37, the complicated relationship between the rheological response and the blend composition is understandable. A close examination of the steady shearing

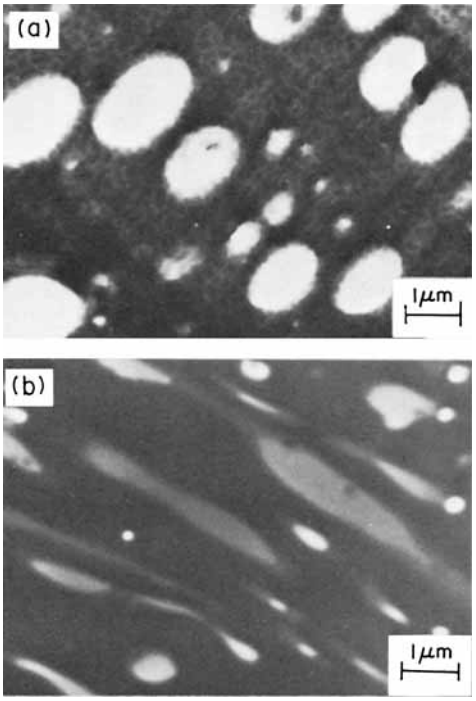

Fig. 36. Photomicrographs for the PS/PMMA=70/30 blend, in which the *dark* area represents the PS phase and the *white* area represents the PMMA phase: (a) before the specimen was subjected to a shearing motion; (b) after the specimen (T = 220°C) was subjected to a shearing motion at $\dot{\gamma}$ = 2.7 s^{-1}.

flow properties (η and $\tau_{11} - \tau_{22}$) given in Figures 29 and 31 reveals that, at high shear rates (or high shear stresses), the PS-rich blends (i.e., PS/PMM=90/10 and PS/PMMA=70/30) tend to give η values lower than, and $\tau_{11} - \tau_{22}$ values higher than, those of the constituent component. Interestingly enough, the PMMA droplets suspended in the continuous PS phase in the PS-rich blends are elongated under a steady shearing deformation, as may be seen in Figures 36 and 37, whereas in the PMMA-rich blends, the PS droplets are not elongated (see Figs. 33 and 34). It can be concluded, therefore, that, in incompatible polymer blends, the deformability of the discrete (droplet) phase greatly influences their bulk rheological properties.

Dependence of the Rheological Properties on the Type of Shearing Flow

It is demonstrated above (see Figs. 1, 2, 9, 10, and 19–22) that the rheological responses of compatible blend systems are independent of the type of shearing flow, i.e., whether steady or oscillatory. However, the situation is quite different for incompatible blend systems. This may be understood if one realizes that the state of dispersion and specifically, the shape of the discrete phase (i.e., droplets) greatly influence the rheological responses of incompatible polymer blends.

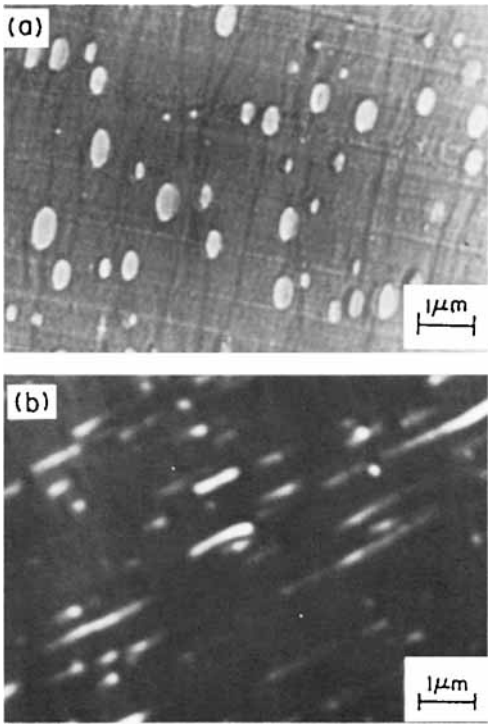

Fig. 37. Photomicrographs for the PS/PMMA=90/10 blend, in which the *dark* area represents the PS phase and the *white* area represents the PMMA phase: (a) before the specimen was subjected to a shearing motion; (b) after the specimen (T = 220°C) was subjected to a shearing motion at $\dot{\gamma}$ = 2.7 s^{-1}.

Consider a spherical droplet suspended in a continuous medium, which is subjected to either a steady shearing flow or an oscillatory shearing flow. Under the steady shearing flow, the droplet is deformed in the direction of the shearing plane, and the greater the shear rate, the longer the droplet will be stretched. On the other hand, under the oscillatory shearing flow, the shape of the droplet will also oscillate, commensurate with the frequency of the oscillation imposed on the fluid. When the droplet phase viscosity is very large compared to the medium viscosity, the oscillatory motion of the cone (or plate) of the rheometer may little affect the shape of the droplet; but when the droplet viscosity is very small compared to the medium viscosity, the shape of the droplet will oscillate greatly. Therefore, one must *not* expect any correlation between η and η' and between $\tau_{11} - \tau_{22}$ and G' for incompatible polymer blends. Indeed, the results shown in Figures 29–32 for the PMMA/PS blend system attest to this fact.

At this juncture, it should be mentioned that the rheological properties of incompatible polymer blends, determined with a capillary rheometer, may *not* be correlatable to those obtained with a cone-and-plate rheometer. This is because the shape of the droplets of a two-phase blend in the fully developed region of a cylindrical tube may be different from that in the constant shearing flow field in a cone-and-plate rheometer. Note that the shearing flow field is *nonuniform* in a capillary, whereas it is *uniform* in a cone-and-plate geometry. Therefore, there is no *a priori* reason to expect that the rheological data determined with

a capillary rheometer should agree with that determined with a cone-and-plate rheometer. This argument can be extended to interpreting the data obtained with the plunger-type capillary viscometer (e.g., an Instron viscometer). As pointed out by Han in his recent article,[19] the shape of the droplets in a two-phase blend, when forced to flow through a plunger-type viscometer, will vary continuously from the upstream end of the reservoir section (i.e., barrel) to a distance from the capillary entrance where fully developed flow is established. Therefore, taking pressure measurements in the reservoir section and making the entrance correction (i.e., Bagley correction) with the data obtained in a plunger-type capillary viscometer would *not* give correct information on the bulk viscosity of incompatible polymer blends.

The authors wish to acknowledge that Werner & Pfleiderer Corporation prepared the blends, using a twin-screw compounding machine.

References

1. H. VanOene, *J. Colloid Interface Sci.*, **40,** 448 (1972).
2. C. D. Han and T. C. Yu, *J. Appl. Polym. Sci.*, **15,** 1163 (1971).
3. C. D. Han and T. C. Yu, *Polym. Eng. Sci.*, **12,** 81 (1972).
4. C. D. Han and Y. W. Kim, *Trans. Soc. Rheol.*, **19,** 245 (1975).
5. C. D. Han, Y. W. Kim, and S. J. Chen, *J. Appl. Polym. Sci.*, **19,** 2831 (1975).
6. Y. W. Kim and C. D. Han, *J. Appl. Polym. Sci.*, **20,** 2905 (1976).
7. C. D. Han, *Rheology in Polymer Processing*, Academic, New York, 1976, Chap. 7.
8. C. D. Han, *Multiphase Flow in Polymer Processing*, Academic, New York, 1981, Chap. 4.
9. J. M. Starita, *Trans. Soc. Rheol.*, **16,** 339 (1972).
10. T. I. Ablazova, M. B. Tsebrenko, A. B. Yudin, G. V. Vinogradov, and B. V. Yarlykov, *J. Appl. Polym. Sci.*, **19,** 1781 (1975).
11. J. S. Noland, H. N. C. Hsu, R. Saxon, and J. M. Schmitt, in *Multicomponent Polymer Systems*, Advanced Chemistry Series, No. 99, Amer. Chem. Soc., Washington, D.C., 1971, p. 15.
12. D. R. Paul and J. O. Altamirano, in *Copolymers, Polyblends, and Composites*, Advanced Chemistry Series, No. 142, Amer. Chem. Soc., Washington, D.C., 1975, p. 371.
13. T. Nishi and T. T. Wang, *Macromolecules*, **8,** 909 (1975).
14. T. K. Kwei, H. L. Frisch, W. Radigan, and S. Vogel, *Macrocolecules*, **10,** 157 (1977).
15. T. T. Wang and T. Nishi, *Macromolecules*, **10,** 421 (1977).
16. C. D. Han, *Rheology in Polymer Processing*, Academic, New York, 1976, Chap. 5 and Appendix B.
17. K. Walters, *Rheometry*, Chapman and Hall, London, 1975.
18. C. D. Han and K. W. Lem, *Polym. Eng.* Rev., **2,** 135 (1982).
19. C. D. Han, Polym. Eng. Rev., **1,** 363 (1981).

Received October 26, 1983
Accepted November 30, 1983